JES, Vol. 52, No. 4, Sept 2024 DOI: 10.21608/JESAUN.2024.289228.1335 Part A: Civil Engineering

Journal of
Engineering Sciences
Faculty of Engineering
Assiut University

JES

مجلة
العلوم الهندسية
كلية الهندسة
جامعة أسيوط

journal homepage: http://jesaun.journals.ekb.eg

Numerical Analysis of CFRP-Confined Circular Concrete Columns under Axial Loading

Received 13 May 2024; Revised 2 August 2024; Accepted 15 August 2024

Mohamed S. Khalafalla [1]

Keywords
Nonlinear analysis, CFRP- Column, Ultimate capacity, Axial stress, Failure mode

Abstract: The axial compression performance of circular columns strengthened with carbon fiber-reinforced polymer (CFRP) was investigated using numerical simulation. The study's objective was to validate a finite element model to match results of experimental testing, to ensure consistent failure modes and load-displacement profiles. The investigation explored the impact of various parameters, including concrete strength, CFRP layer numbers, slenderness ratio, steel reinforcement ratio, and cross-sectional area, on CFRP column behavior. The analysis revealed valuable insights into stress-strain relationships and ultimate load-bearing capacity. This study provides vital information for structure engineering practices and design strategies in the industry, highlighting the significance to utilize CFRP technology to enhance structural performance, especially the consistent stress distribution on the concrete core. To understand the mechanical response of CFRP circular concrete columns, engineers can optimize design and construction techniques to create more efficient and durable structures elements, ultimately to improve public safety and to reduce maintenance processes.

1. Introduction

Infrastructure engineers consistently aim to streamline the construction phase to enhance the mechanical properties and long-term durability of structures [1]. In regions prone to earthquakes, it is imperative to strengthen existing buildings to mitigate risks and address deficiencies where it is widely acknowledged. A notable approach involves circumnutating columns with high-

[1] Assistant Professor-Construction Research Institute, NWRC-Egypt

https://doi.org/10.21608/JESAUN.2024.289228.1335

strength fiber-reinforced polymer such as Carbon Fiber Reinforced Polymer (CFRP) tube, offers substantial improvements in both the permeability and structural elements axial capacity. This method provides longitudinal reinforcement and enhances shear capacity through strengthening with external jacket. The integration of advanced polymer composites in construction has experienced rapid growth since the year 2000, instilling greater confidence in engineers regarding the materials' potential. This confidence has resulted in increased utilization, particularly in the reinforcement of buildings [2].In order to improve ductility and strength for columns, particularly those with circular sections, confinement with Fiber-Reinforced Polymer (FRP) is implemented, The FRP jacket provide

Nearly unvarying circumnutating to the concrete under axial load. While wide research has been conducted on the performance of FRP-confined concrete, prevailing physical and theoretic studies have predominantly focused on comprehending and modeling unreinforced concrete columns subjected to axial loads. These investigations encompass various stress-strain models for FRP-confined concrete, comprising models designed for practical applications [3] as well as those tailored for analytical purposes [4]. Columns are usually exposed to axial load and bending moment. Even a column proposed to carry concentric stress needs to be designed to resist moments generated from a different case, geometric/material shortages, and unlooked-for load eccentricities especially. To account for the influence of eccentric loading and column slenderness, many codes incorporate an extra load eccentricity into structural analysis.

Studies explored the Concrete Filled FRP Tube (CFFT) method as a viable replacement of steel reinforced concrete columns, this highlights the FRP tubes multifaceted benefits, including its dual role as both longitudinal and transverse reinforcement its ability to function as a structural formwork and provide corrosion resistance. [5]. The implementation of fiber-reinforced polymer (FRP) composites has been gaining popularity in recent years due to their high strength-to-weight ratio, corrosion resistance, and versatility. [6]. A limited number of studies have been conducted to investigate the flexural behavior of concrete-filled fibre-reinforced polymer (FRP) tubes, which is essential to understand the structural performance of these innovative materials in various applications. The available literature on FRP-confined concrete columns currently is limited to the study of short columns under eccentric loading, while the effect of slenderness on these columns has been investigated by limited studies. [7, 8]. The behavior of FRP-confined square or rectangular columns under eccentric loading has not been thoroughly investigated. [9]. The majority of the existing studies on FRP-confined slender circular concrete columns utilized specimens with diameters ranging from 150 to 205 mm. [10]. Past experimental studies have suggested that there may be performance disparities between small and tall FRP-confined concrete columns, particularly for FRP-confined rectangular concrete columns. [11]. As a result, there are uncertainties associated with the extrapolation of small-scale sample results to larger-scale FRP-confined RC columns, as previous studies have demonstrated. Therefore, there is a significant need for further experimental research on larger FRP-confined slender RC columns

under various loading conditions.

Several design standards and guidelines to strengthen RC structures with FRP are currently available and offer provisions to design against the axial-bending interaction in eccentrically loaded columns, as exemplified by the Concrete Society [12] Provide design models to estimate the capacity loads of FRP-confined slender RC columns. However, these models have been developed based on experimental studies conducted on small-scale column specimens. The novelty of this study lies in the extensive scope of the study. It covers 45 test cases with various parameters, including slender ratios, CFRP layers numbers, and concrete strength-to-steel ratio. This allows the comprehensive analysis of the behavior of CFRP-confined concrete columns under axial compressive loading. While previous studies have investigated similar topics, the sheer number of test cases and variables considered in this study provides a more detailed understanding of the complex interactions between these parameters and their impact on the performance of CFRP-confined columns.

2. Data Used

The total specimens were 45 columns specimens divided into 2 Groups, Group-1 had 28 columns depending on previous experimental work, 24 were verified numerically. Group 2 has 17 specimens that were investigated as Finite element models with the same properties as group 1. The test program had been reported exactly depending on three studies Ilki et.al. (2008) [13], Wang et al. (2012) [14], and Al-Nimry and Soman (2018) [15] under axial compression stress.
Twenty columns from Wang et al. (2012) study [14], were designated with code letter C, defining the "circular" column, with numbers 1 or 2 to denote different column diameters. The second letter H represents the volumetric ratio of ring steel, with subsequent numbers to indicate 0% plain concrete, 0.5%, and 1.0% reinforcement. The third letter L denotes the number of CFRP wrap layers. Four samples from the Ilki et.al. 2008 [13] study was conducted using code LSR/NSR referring to the Low and Normal concrete strength respectively, C: circular column, followed by the spacing distance between stirrups and number of warped CFRP layers.
Al-Nimry and Soman’s 2018 study [15] conducted four column samples. The test specimens were divided into two groups C1 and C2: 1175 mm length and 19.6 slenderness ratio (kl/r); and 800 mm length and 13.3 a kl/r ratio respectively. The second code letter S1 and S2 refer to the spacing of 6-mm diameter stirrups: 125 mm and 187.5 mm respectively. The last letter of code 1C: denotes one layer of CFRP. Previous works are summarized in Table 1 the corresponding experimental investigation program was conducted under the same boundary conditions as reported by the authors. The axial compression via displacement performance of specimens was tested and analyzed to assess the CFRP behavior as strengthening.

Table 1: Total of Sample Data Description

No	Code	Author	D (mm)	H (mm)	unconfined Strength (Mpa)	No. Of CFRP Layers	Longitudinal steel		Spirals steel	
							No. Bars	Diameter (mm)	Diameter (mm)	S (mm)
1	C2H0L1M-G1	Wang et al. (2012)	204	612	24.50	1	0	0	0	0.00
2	C2H0L1C-G1		204	612	24.50	1	0	0	0	0.00
3	C2H0L2M-G1		204	612	24.50	2	0	0	0	0.00
4	C2H0L2C-G1		204	612	24.50	2	0	0	0	0.00
5	C1H0L1M-G1		305	915	24.50	1	0	0	0	0.00
6	C1H0L2M-G1		305	915	24.50	2	0	0	0	0.00
7	C1H1L1M-G1		305	915	24.50	1	8	12	6	80.00
8	C1H1L1C-G1		305	915	24.50	1	8	12	6	80.00
9	C1H1L2M-G1		305	915	24.50	2	8	12	6	80.00
10	C1H1L2C-G1		305	915	24.50	2	8	12	6	80.00
11	C1H2L1M-G1		305	915	24.50	1	8	12	6	40.00
12	C1H2L2M-G1		305	915	24.50	2	8	12	6	40.00
13	C2H1L1M-G1		204	612	24.50	1	6	10	6	120.00
14	C2H1L1C-G1		204	612	24.50	1	6	10	6	120.00
15	C2H1L2M-G1		204	612	24.50	2	6	10	6	120.00
16	C2H1L2C-G1		204	612	24.50	2	6	10	6	120.00
17	C2H2L1M-G1		204	612	24.50	1	6	10	6	60.00
18	C2H2L1C-G1		204	612	24.50	1	6	10	6	60.00
19	C2H2L2M-G1		204	612	24.50	2	6	10	6	60.00
20	C2H2L2C-G1		204	612	24.50	2	6	10	6	60.00
21	NSR-C-050-3-G1	Ilki et al. (2008)	250	500	27.58	3	6	10	8	50.00
22	NSR-C-100-3-G1		250	500	27.58	3	6	10	8	100.00
23	NSR-C-145-3-G1		250	500	27.58	3	6	10	8	145.00
24	LSR-C-145-3-G1		250	500	14.83	3	6	10	8	145.00
25	C2-S1-1C-G1	Al-Nimry and Soman (2018) /Abaqus	192	800	41.00	1	6	10	6	125.00
26	C2-S2-1C-G1		192	800	41.00	1	6	10	6	187.50
27	C1-S1-1C-G1		192	1175	41.00	1	6	10	6	125.00
28	C1-S2-1C-G1		192	1175	41.00	1	6	10	6	187.50
29	C2H0L1M-G2	Abaqus (2022)	204	612	41.00	1	0	0	0	0.00
30	C2H0L2M-G2		204	612	41.00	2	0	0	0	0.00
31	C1H0L1M-G2		305	915	41.00	1	0	0	0	0.00
32	C1H0L2M-G2		305	915	41.00	2	0	0	0	0.00
33	C1H1L1M-G2		305	915	41.00	1	8	12	6	80.00
34	C1H1L2M-G2		305	915	41.00	2	8	12	6	80.00
35	C1H2L1M-G2		305	915	41.00	1	8	12	6	40.00
36	C1H2L2M-G2		305	915	41.00	2	8	12	6	40.00
37	C2H1L1M-G2		204	612	41.00	1	6	10	6	120.00
38	C2H1L2M-G2		204	612	41.00	2	6	10	6	120.00
39	C2H2L1M-G2		204	612	41.00	1	6	10	6	60.00
40	C2H2L2M-G2		204	612	41.00	2	6	10	6	60.00
41	C1H0L3M-G2		305	915	41.00	3	0	0	0	0.00

No	Code	Author	D (mm)	H (mm)	unconfined Strength (Mpa)	No. Of CFRP Layers	Longitudinal steel		Spirals steel	
							No. Bars	Diameter (mm)	Diameter (mm)	S (mm)
42	C2-S1-1C-G2	Al-Nimry and Soman (2018) /Abaqus	192	800	24.50	1	6	10	6	125.00
43	C2-S2-1C-G2		192	800	24.50	2	6	10	6	187.50
44	C1-S1-1C-G2		192	1175	24.50	1	6	10	6	125.00
45	C1-S2-1C-G2		192	1175	24.50	2	6	10	6	187.50

3. Finite Element Model

The finite element program ABAQUS was employed to simulate the numerical model depicted in Figure 1, to examine the CFRP performance as a column strengthening measure. The C3D8R element was utilized to model the concrete, with the T3D2 element representing the steel bars and stirrups as two-dimension element with compression/tensile strength. The S4R shell element was used to simulate the CFRP, while the rigid solid plates were positioned at both ends of the column to facilitate the uniform transfer of axial loads. A mesh size of D/20 was set to achieve a reasonable balance between solution accuracy and computational time. The tie interaction "surface-to-surface" contact model was employed to simulate the full connection between the rigid plates and the column surfaces, with the upper plate's longitudinal displacement released and the freedoms constrained in other directions. The lower plate was fully constrained, and the axial load was simulated using a displacement-controlled model.

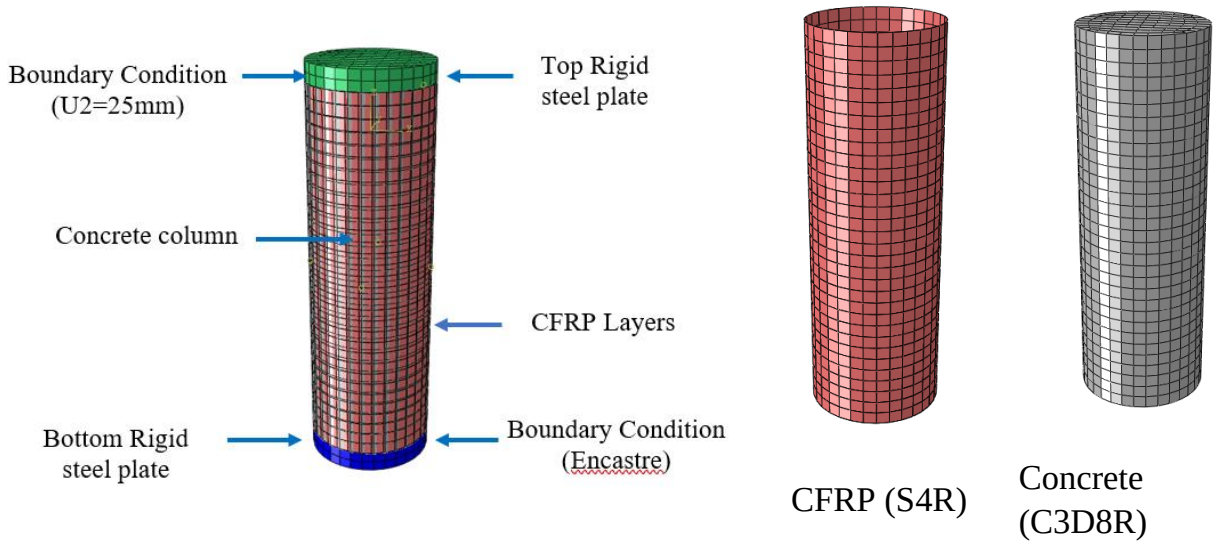

Fig. 1. Finite element model for CFRP columns.

3.1 Confined concrete

The core concrete is warped by a CFRP sheet. The interaction between the CFRP sheet and concrete can be discounted at the initial stage. The concrete properties in the elastic stage were settled by the elasticity modulus ($E_c = 4400\sqrt{fc'}$) and Poisson's ratio (υ =0.2) as recommended in ACI 318. The interaction generated between the concrete and CFRP sheet is due to the expansion of concrete at the plastic stage. The infilled concrete is modeled using the concrete-damaged plasticity model (CDPM) in ABAQUS. The CDPM is set in terms of three factors the yield surfaces which are described by the compressive strength, tension strength, and the plastic flow potential of concrete which set by the flow potential eccentricity (e), the dilation angle (ψ), The biaxial loading to uniaxial loading (f_{bo} /fco), the tensile peak to the compressive peak which is called the second stress constant (K), and Viscosity parameter is last factor. The tension damage and fracture energy are variable due to experimental specimens and references until matched.

Table 2: Concrete Damage Plasticity Model

Dilation angle (ψ)	Eccentricity (e)	Fbo/fco	K	Viscosity parameter
30	0.01	variable	0.667	1E-6

3.2 CFRP

The CFRP material has high tensile strength and exhibits an elastic behavior in the longitudinal direction but ignored compressive strength. "LAMINA" is the material type used for CFRP behavior. The tensile fracture is the mode failure of zero angle CFRP, so the damage should be measured. The elasticity, damage evaluation, and peak strength are certainly defined for composite fiber. The elastic modulus parameters are set as 142GPa, and 10.3GPa in longitudinal and transfer directions respectively [19].

4. Model Verification

4.1 Typical Failure Modes

By comparing the numerical results with the test data through the Tsai-Wu failure model (measure failure at integration point), the accuracy of the finite element model has been validated. The comparison between numerical simulations and experimental results is demonstrated in Figure 2, using specimen C1H0L2M, LSR-C-145-3, and C1-S2-1C-A as references. The failure mode exhibits a high degree of consistency, with the curves of the specimens reaching the peak load at failure Nu. Nevertheless, the peak points in numerical simulations and experimental tests display distinct displacements.

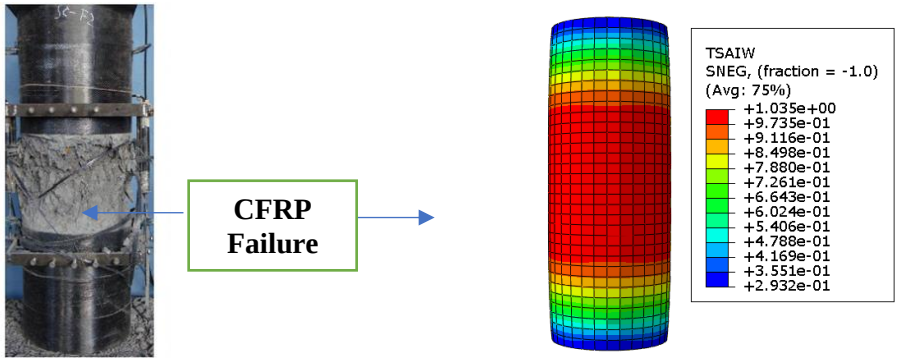

A. CFRP Failure (C1H0L2M)

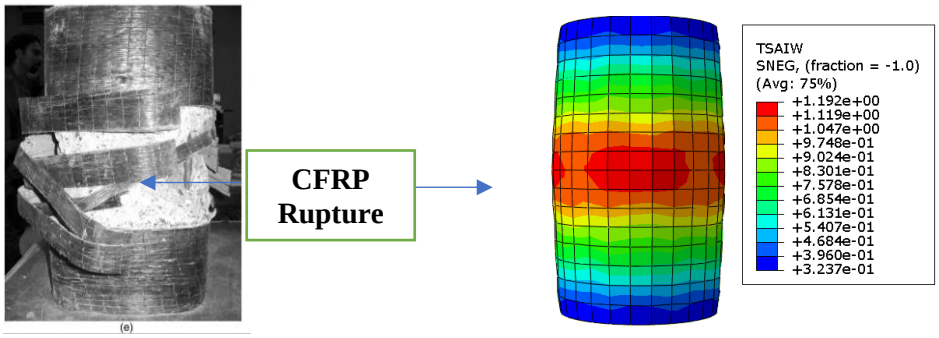

b. CFRP Rupture (LSR-C-145-3)

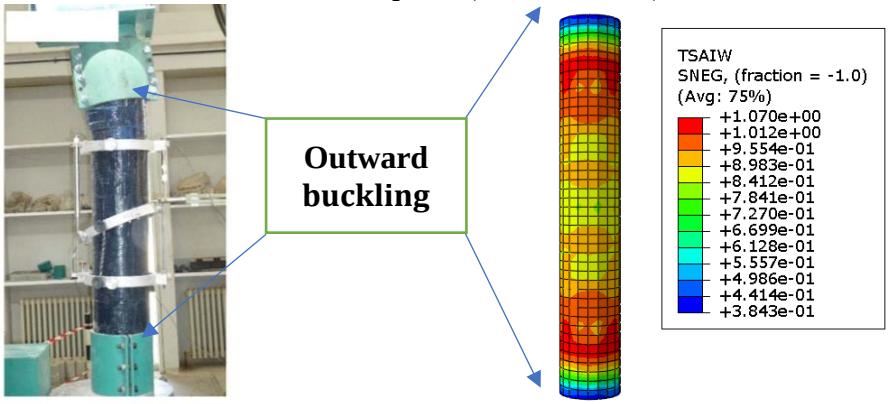

c. outward buckling (C1-S2-1C-A)

Figure 2: Typical failure modes of CFRP specimens compared.

4.2 Load-Strain Curves

The load-strain curves obtained by the Finite Element Model (FEM) and experimental data are compared. It was obvious that the behaviors were highly consistent (**Figure 3**). This means the model mesh is of the optimum size used. The gaps between CFRP and concrete could delay the CFRP contribution to achieve larger deformability before failure [20]. The peak value of load (Nu) of FEM and experimental were compared and the error comparison between them is shown in **Table 3**, It resulted in the mean ratio (Nu,FE/Nu) of 1.022 with a standard deviation of 0.06. In general, the finite element model shows a high consistency with experimental results in terms

of failure mode, load-strain curves, and ultimate capacity. The failure is sudden after CFRP separates, ruptures, or outward buckling, where the CFRP fails. This mode of failure matches experimental and numerical due to the tensile stresses of CFRP reaching the peak.

Table 3: Comparison between loading capacity

No	Code	Unconfined Strength (Mpa)	No. Of Layers	Tested Concrete Strength fcc' (Mpa)	Tested Loading (KN)	FEM Loading (KN)	Loading percentage
1	C2H0L1M-G1	24.500	1.000	46.100	1507.391	1471.030	0.976
2	C2H0L1C-G1	24.500	1.000	42.300	1383.137	1471.030	1.064
3	C2H0L2M-G1	24.500	2.000	65.200	2131.928	2365.660	1.110
4	C2H0L2C-G1	24.500	2.000	66.800	2184.245	2365.660	1.083
5	C1H0L1M-G1	24.500	1.000	35.000	2558.188	2496.460	0.976
6	C1H0L2M-G1	24.500	2.000	55.300	4041.936	3954.040	0.978
7	C1H1L1M-G1	24.500	1.000	41.500	3033.279	3044.070	1.004
8	C1H1L1C-G1	24.500	1.000	43.100	3150.225	3044.070	0.966
9	C1H1L2M-G1	24.500	2.000	52.200	3815.354	3980.090	1.043
10	C1H1L2C-G1	24.500	2.000	61.800	4517.028	3980.090	0.881
11	C1H2L1M-G1	24.500	1.000	47.000	3435.280	3598.200	1.047
12	C1H2L2M-G1	24.500	2.000	62.100	4538.956	4744.410	1.045
13	C2H1L1M-G1	24.500	1.000	52.100	1703.581	1666.900	0.978
14	C2H1L1C-G1	24.500	1.000	49.900	1631.644	1666.900	1.022
15	C2H1L2M-G1	24.500	2.000	66.100	2161.357	2469.490	1.143
16	C2H1L2C-G1	24.500	2.000	68.900	2252.912	2469.490	1.096
17	C2H2L1M-G1	24.500	1.000	52.200	1706.851	1698.430	0.995
18	C2H2L1C-G1	24.500	1.000	57.000	1863.802	1698.430	0.911
19	C2H2L2M-G1	24.500	2.000	69.500	2272.531	2388.060	1.051
20	C2H2L2C-G1	24.500	2.000	75.000	2452.371	2388.060	0.974
21	NSR-C-050-3-G1	27.580	3.000	77.590	3810.223	3965.450	1.041
22	NSR-C-100-3-G1	27.580	3.000	72.600	3565.179	3668.200	1.029
23	NSR-C-145-3-G1	27.580	3.000	71.950	3533.259	3562.250	1.008
24	LSR-C-145-3-G1	14.830	3.000	54.680	2685.179	2709.780	1.009
Mean							**1.017**
Standard division							**0.058**

5. Analysis

5.1 Typical stress-strain Curve

The typical stress-strain curve of the CFRP-confined concrete specimen is investigated using experimental and numerical models. The behavior is delivered into four parts. The first part

corresponds to a stress-strain curve that is identical to the approved unconfined concrete, featuring a parabolic initial segment and a subsequent linear region, Figure 4. The second part acknowledges the fact that the initial stiffness of confined concrete is unaffected by the CFRP due to passive warping, resulting in an identical initial slope (Ec) to that of unconfined concrete. The third part represents the activation of CFRP confinement when the concrete behavior becomes non-linear, thus affecting the non-linear portion of the first part. The fourth part confirms a smooth stress-strain curve, with the parabolic first part merging seamlessly into the linear second part (there is no discontinuity in slope between the two sections).

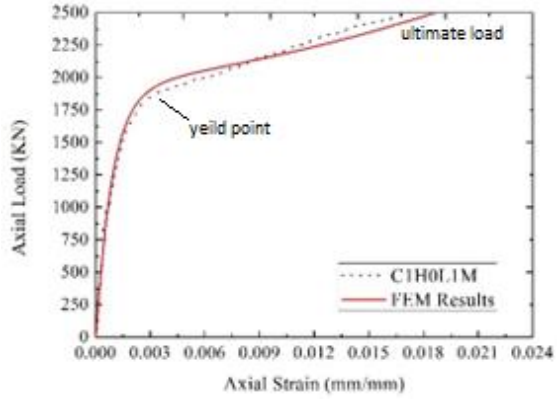

3.1: C1H0L1M

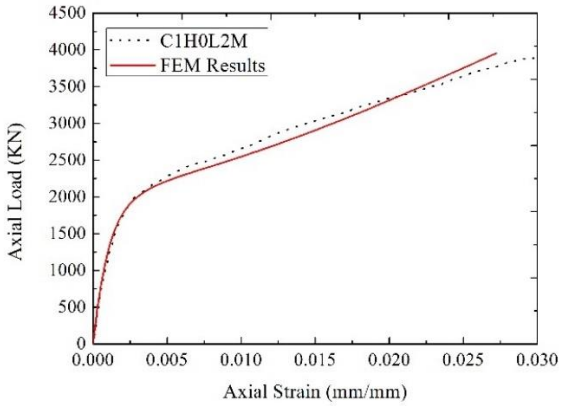

3.2: C1H0L2M

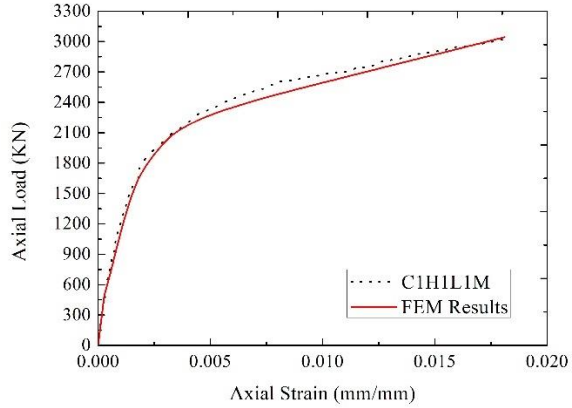

3.3: C1H1L1M

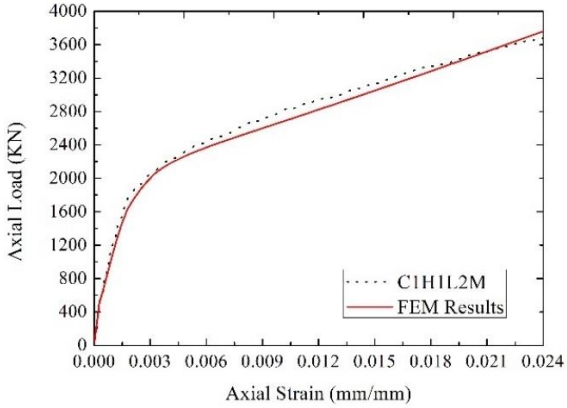

3.4: C1H1L2M

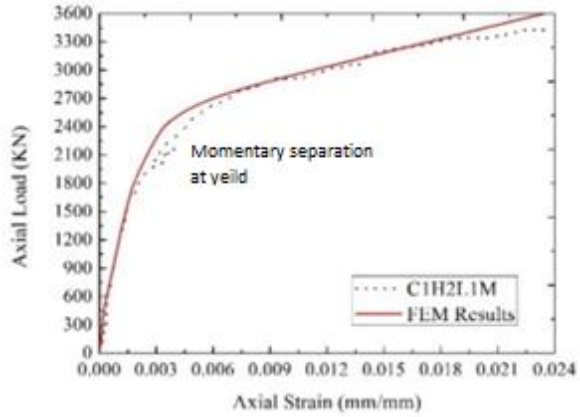

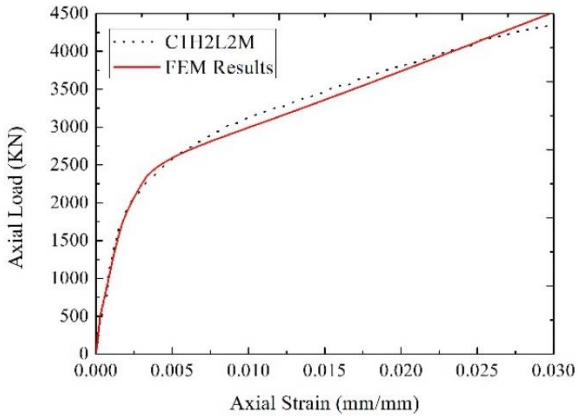

3.5: C1H2L1M

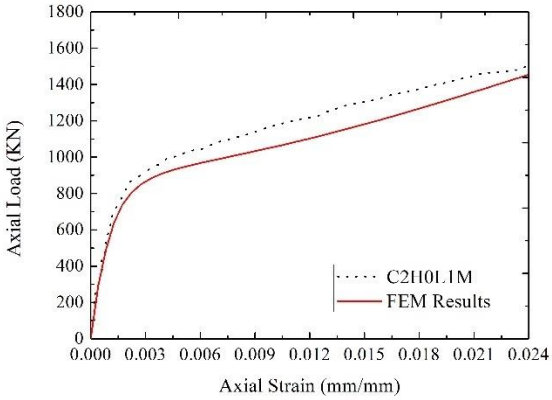

3.6: C1H2L2M

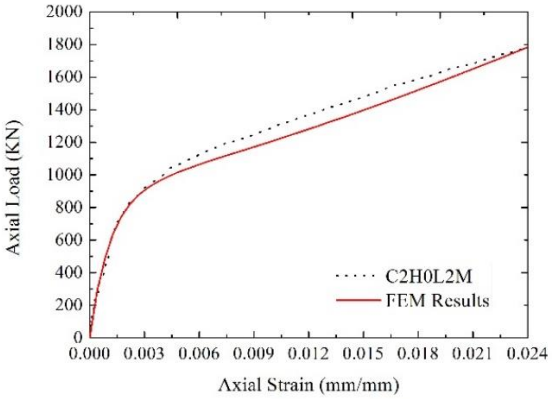

3.7: C2H0L1M

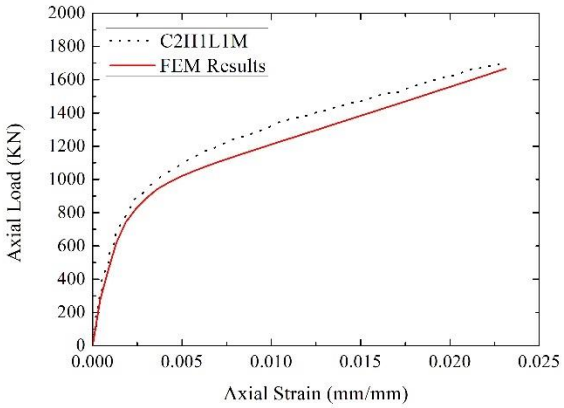

3.8: C2H0L2M

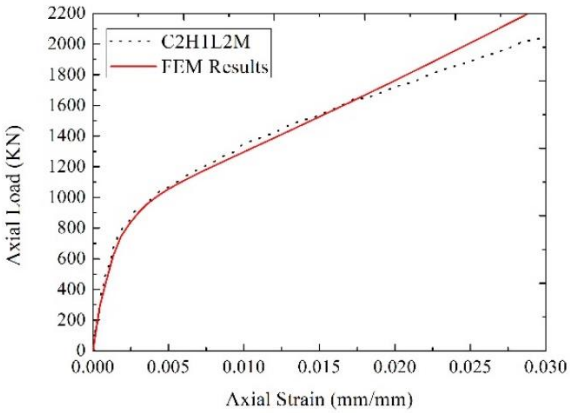

3.9: C2H1L1M

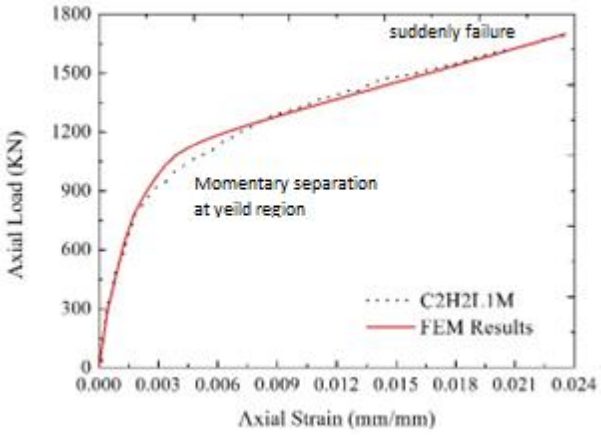

3.10: C2H1L2M

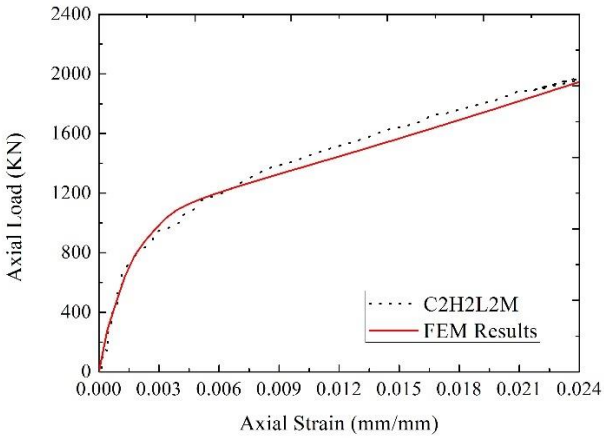

3.11: C2H2L1M

3.12: C2H2L2M

Figure 3: Comparison between experimental and finite element load-strain curves of CFRP specimens.

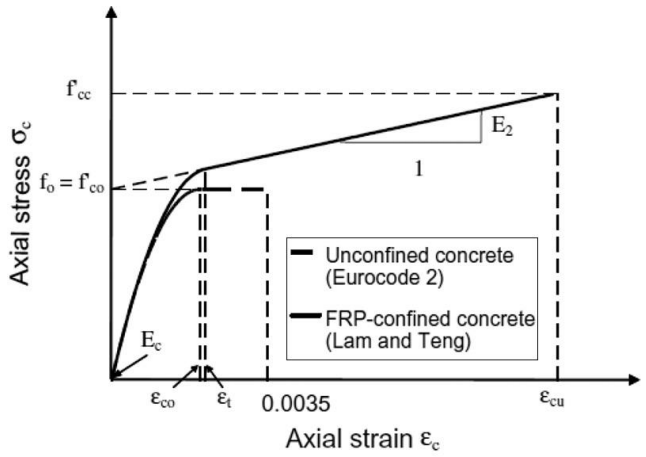

Figure 4: Typical stress-strain curve of CFRP confined concrete. [9]

5.2 Parameter Analysis

The parameters of CFRP specimens were investigated to encompass the Internal Steel Reinforcement, Slenderness Ratio, Specimen Size, and concrete strength.

5.2.1 Internal Steel Reinforcement

The core concrete is warped by the internal spiral and longitudinal reinforcing steel as part of an FRP jacket system. In this investigation, the confinement provided by the stirrups was estimated using the expressions formulated by Mander et al. [21].

$$f_{cc} = f'_{co}\left(-1.254 + 2.54\sqrt{1 + \frac{7.94 f'_l}{f'_{co}}} - 2\frac{f'_l}{f'_{co}}\right) \qquad \text{Eq. (1)}$$

Where $\boldsymbol{f_{cc}}$ the steel-confined concrete compression strength,

f'_{co} The unconfined concrete compressive strength.

f'_l Effective lateral constraining pressure.

$$f'_l = 0.5\, k_e \rho_s f_{yh} \qquad \text{Eq. (2)}$$

In which, k_e is the confinement effectiveness constant for spiral given by Eq. (3), ρ_s Is the volumetric ratio between the transverse confining steel to confined concrete core from Eq. (4), f_{yh} Is the yield strength of spiral reinforcement.

$$k_e = \left(1 - \frac{s'}{2d_s}\right)^2 / \left(1 - \rho_{cc}\right) \qquad \text{Eq. (3)}$$

Where s' is the clear vertical spacing between the transverse bars, d_s Is the diameter of the spiral, ρ_{cc} is the ratio between the longitudinal reinforcement cross section to the area of the concrete.

$$\rho_s = \frac{4\,A_{sp}}{d_s\,S} \qquad \text{Eq. (4)}$$

Where A_{sp} is the area of the reinforcement, S is the spacing of the spiral center-to-center.

The stress-strain curves revealed that the internal steel's properties were primarily influenced by the number of CFRP layers, as observed by Wang et al [14]. The effect of a constant number of CFRP layers but with different reinforcement volumetric ratios on the stress-strain response is shown in **Figure 5.** The specimens with a minimum number of CFRP layers (one layer of CFRP) had an increased ductility capacity increased upon an increase in reinforcement ratio. The softening area under the curve is also (refer to **Figure 5a**) enhanced by the increase in the steel ratio. Whereas the samples warped with two layers of CFRP, there was no significant effect of reinforcement. In addition, the softening area under the stress-strain curve is increased upon the addition of reinforcement. In general, the confinement stresses delivered by the reinforcement and CFRP layers have become inefficient with an increase in the number of CFRP wrap layers. Whereas the simulate of Ilki et.al. [13] Study indicates that the small spacing (45) mm between stirrups has a higher loading capacity where the (100 and 145) mm converged and decreased in loading capacity.

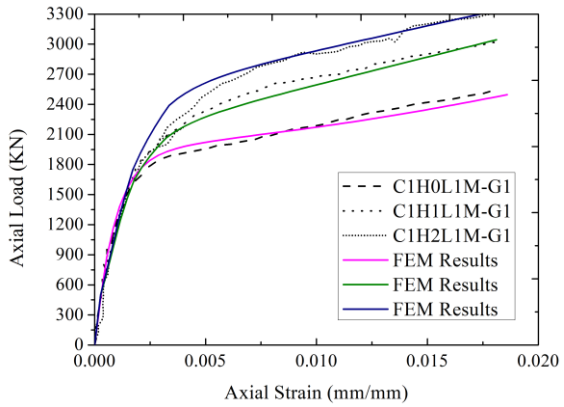

Figure 5. a: Greater cross-section and One Layer of CFRP

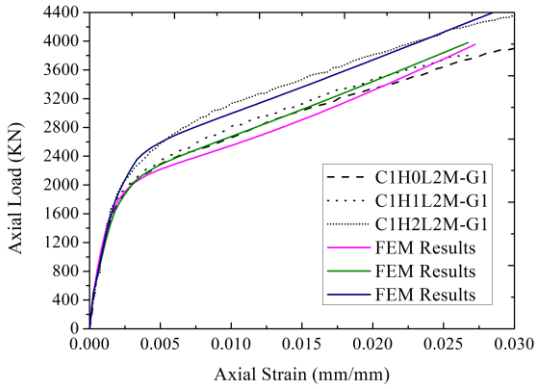

Figure 5. b: Greater cross-section and two Layer of CFRP

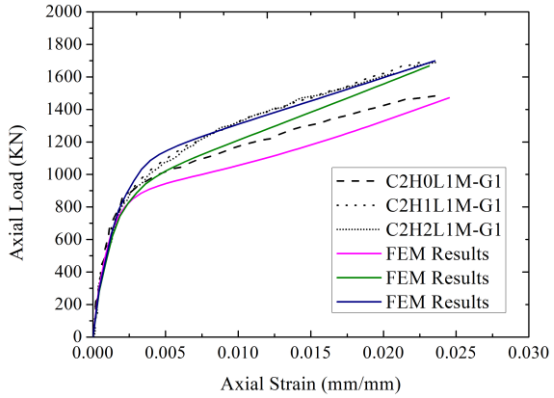

Figure 5. c: Smaller cross-section and One Layer of CFRP

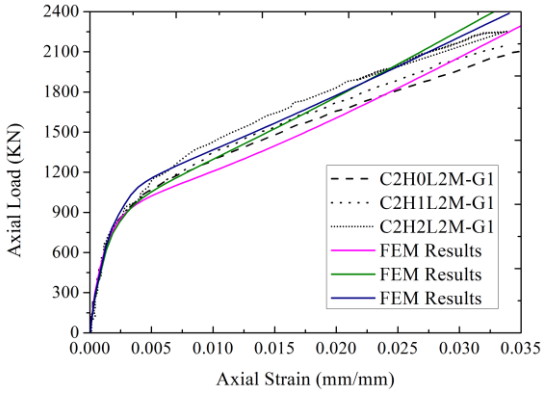

Figure 6.d: Smaller cross-section and two Layer of CFRP

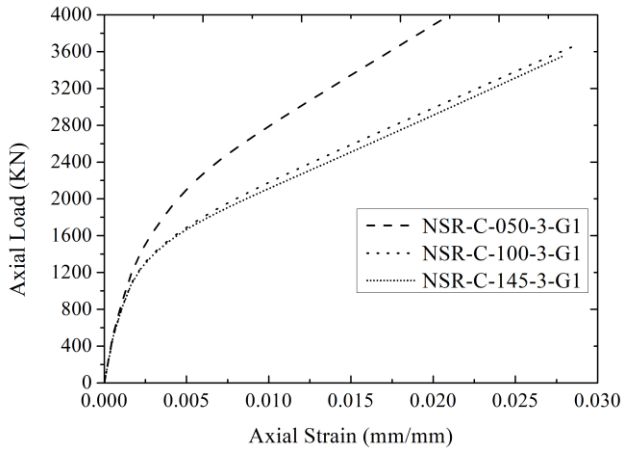

Figure 5. f: Different spacing of Stirrups

Figure 5: Effect of internal steel on Load-Strain curve

6. Effect of Specimen Size

The axial stress-strain curves indicated that the cross-section mainly affects the ultimate capacity. As the column's diameter increases, the CFRP wrap effect is reduced. The strength of the columns is lost only when the wrap fractures. The residual strength made available by the columns cross-section allows stress to be released slowly. The influence of the cross-section area on compression stress and axial strain of CFRP specimens was studied as shown in Figure 6 for group 1 and 2. The behavior was indicated by comparing specimens at no steel. The results show that with the decrease in column diameter from 305 to 204 cm, the axial compression strength increases by 28.7% whereas the ultimate strain improved by 33.8%. The cross-sectional area exhibited a counterintuitive relationship with the ductility and specimens' energy absorption, regardless of whether they were reinforced with one or two layers of CFRP.

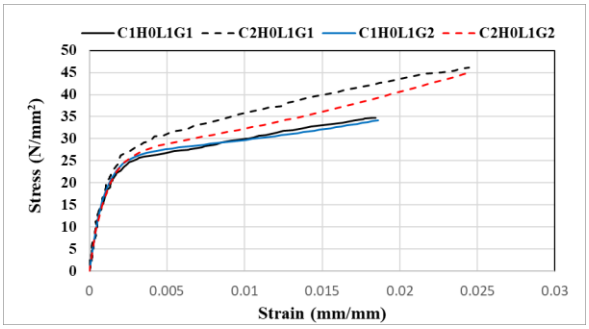

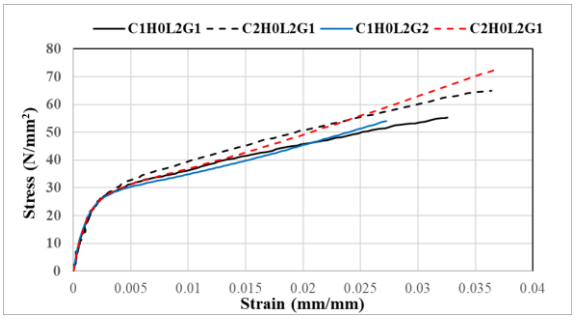

Figure 6. a: Stress-Strain Curve at 1-layer of CFRP

Figure 6. b: Stress-Strain Curve at 2-layer of CFRP

Figure 6: Effect of Specimens Size on Stress-Strain curve

7. Effect of Slenderness ratio

Figure 7 depicts the axial load and strain values of CFRP specimens with diameter-to-thickness ratios of C1 (h = 1175mm, kl/r = 19.6) as a long column, and C2 (h = 800mm, kl/r = 13.3) as a short column and spacing between stirrups S1 (125mm) and S2 (187.5mm) depend on Al-Nimry and Soman 2018 study. The limiting slenderness ratios value, as determined by Eq. (5) [3], decrease significantly when columns are reinforced with single and double layers of CFRP, as calculated using the confined concrete strengths derived from Eq. (6). Consequently, the secondary moments will affect the C1 columns, when they are contained by the FRP sheets. The original slenderness of the columns (kl/r = 13.3), which remains below the modified limit of 19, indicates that the FRP confinement of C2 columns does not introduce additional slenderness-related effects. The test results revealed that the unconfined C2 columns did not exhibit buckling behavior, whereas the FRP-confined C2 columns displayed clear buckling signs. Furthermore, the C1 specimens, which were slenderer, exhibited more pronounced buckling compared to the shorter C2 specimens.

$$\lambda_{cc} = \lambda_c \sqrt{\frac{f'_{co}}{f'_{cc}}} \qquad \text{Eq. (5)}$$

$$f'_{cc} = f'_{co} + \psi_f * 3.3\ k_a f_l \qquad \text{Eq. (6)}$$

Where: ψ_f is a reduction constant equal to 0.95 , K_a is the efficiency factor 1 for circular sections. The axial strength increased slightly as the slenderness ratio decreased. Steel tie spacing in specimens has no effect on loading or strain capacity. Figure 2.c depicts the effect of the slenderness proportion on the beginning of the failure pattern.

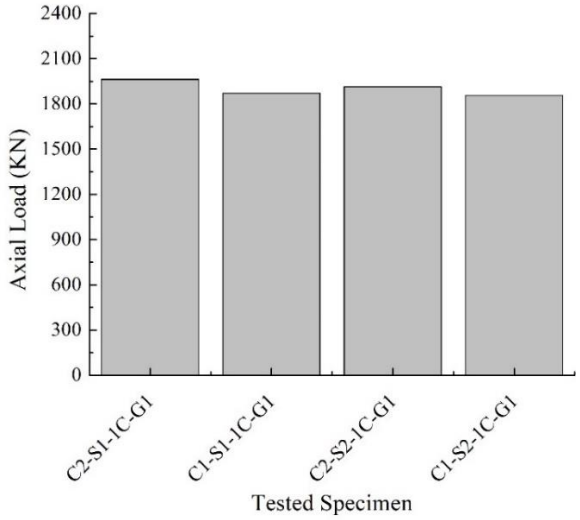

Figure 7. a: Load Capacity

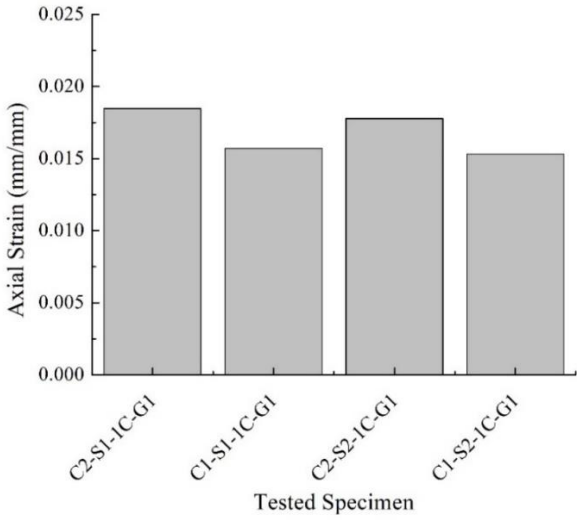

Figure 7. b: Strain Capacity

Figure 7: Effect of Slenderness Ratio on Loading and Strain

8. Effect of concrete strength

The concrete strength affects the CFRP performance. The low-strength concrete has axial and centrifugal strain before others, which provides for the CFRP sheet to establish confinement early. Whereas the axial capacity section increased by 23.12% at high-strength concrete, the ultimate strain decreased by 19.04% to normal strength on average. Accordingly, high-strength concrete has a low ductility behavior. **Figure 8** provides a stress-strain curve comparison between experimental and theoretical by normal strength in G1 and high strength in G2 in the Wang et al. [14] study and low/normal strength in the llki et al. [13] Study, respectively. The compressive strength, ultimate bearing capacity, and elastic stiffness of the CFRP specimens were significantly enhanced. It was observed that the higher the unconfined concrete strength, the lower the effect of the fiber. Where the Low-strength unconfined concrete improved by 57.75% while high-strength concrete improved by only 30.09%.

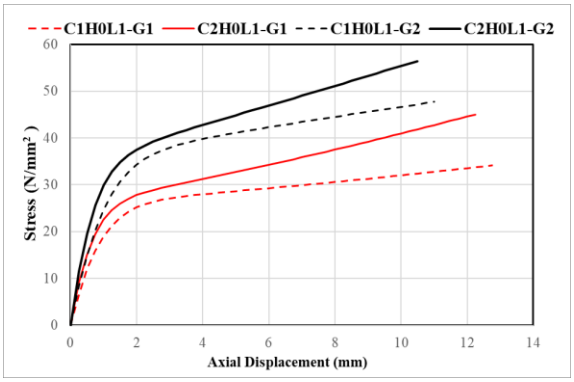

Figure 8.a: Stress-disp. Curve (Wang et.al. 2012)

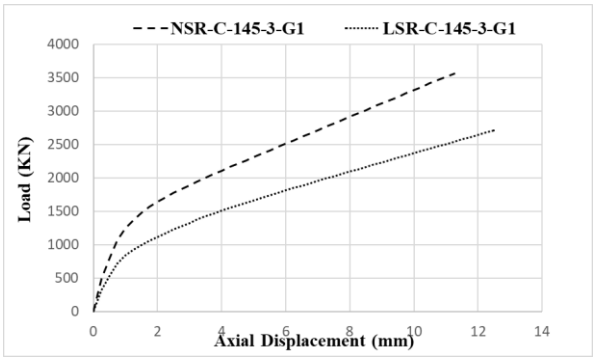

Figure 8.b: Load-disp. Curve (Ilki et.al. 2008)

Figure 8: Effect of Concrete Strength on section capacity

9. Conclusions

The behavior of concrete under contact stress between CFRP and columns. The stress-strain response of various relevant parameters was investigated using numerical simulations of carbon fiber-reinforced polymer (CFRP) specimens. Furthermore, an assessment and comparison to prevail behavior formulas to predict ultimate axial capacity were undertaken. The ensuing conclusions were derived from the numerical simulations:

1. A finite element analysis (FEA) model accurately predicted the behavior of composite specimens under axial compression, matching experimental results in terms of failure mode, load-deformation response, ultimate bearing capacity, and steel strain development.
2. Initially, concrete did not exhibit noticeable contact stress, with plastic flexion of steel occurring after the elastic zone.
3. As concrete reached its plastic limit, contact stress between CFRP layers and concrete increased, leading to local or complete CFRP fracture upon exceeding the allowable spiral

strain.

4. The FEA showed consistent stress distribution within the core concrete, exceeding its compressive strength, and elevated compression strength in concrete reduced specimen ductility, while CFRP with higher tensile strength improved axial compressive characteristics. While the column's diameter increases, the CFRP wrap effect is reduced. and the strength of the columns is lost only when the wrap fractures
5. The softening area under the curve enhanced by the increase in the amount of steel ratio, but the confinement stresses delivered by the reinforcement and CFRP layers have become inefficient with an increase in the number of layers of CFRP wrap.
6. As confinement stress increases, the likelihood of column buckling grows, particularly for columns with high slenderness ratios. And it also noted that the higher the unconfined concrete strength, the lower the effect of the fiber

Reference

[1] L.H. Han, W. Li, R. Bjorhovde, Developments and advanced applications of concrete-filled steel tubular (CFST) structures: members, Journal of Constructional Steel Research 100, (2014) 211–228. http://dx.doi.org/10.1016/j.jcsr.2014.04.016

[2] L. C. Hollaway, and J. G. Teng. 2008. Strengthening and rehabilitation of civil infrastructures using fibre-reinforced polymer (FRP) composites. (2008), Hardback ISBN: 9781845694487, eBook ISBN: 9781845694890, Netherlands: Elsevier.

[3] L. Lam, and J. G. Teng. "Design-oriented stress–strain model for FRP-confined concrete." Construction and Building Materials, (2003), 471–489. https://doi.org/10.1016/S0950-0618(03)00045-X

[4] J. G. Teng, G. Lin, and T. Yu. 2015. "Analysis-oriented stress-strain model for concrete under combined FRP-steel confinement. (2014), Journal Composite Construction. 04014084 (1-14).

[5] https://doi.org/10.1061/(ASCE)CC.1943-5614.0000549

[6] A. Mirmiran, M. Shahawy, Behaviour of concrete columns confined by fiber composites, J. Structural Engineering, (1997), 123 (5), 583–590. https://doi.org/10.1061/(ASCE)0733-9445(1997)123:5(583)

[7] M.N.S. Hadi, W. Wang, M.N. Sheikh, Axial compressive behavior of GFRP tube reinforced concrete columns, Construction and Building Materials, (2015), 81, 198–207. http://dx.doi.org/10.1016/j.conbuildmat.2015.02.025

[8] Bernat Csuka, and Laszlo P. Kollár. "FRP-confined circular columns subjected to eccentric loading. Journal of Reinforced Plastics and Composites, (2011), 30 (14): 1167–1178. https://doi.org/10.1177/0731684410397844

[9] Ghali, K., S. Rizkalla, M. Kassem, T. Fawzy, and M. Mahmoud.2003. "FRP-confined circular columns under small eccentric loading." In Proc., 5th Alexandria Int. Conf. on Structural and Geotechnical Engineering, 20–22. Alexandria, Egypt: Alexandria University.

[10] Muhammad N.S. Hadi, and Ida Bagus Rai Widiarsa... "Axial and flexural performance of square RC columns wrapped with CFRP under eccentric loading." journal of composites for construction. (2012), 16 (6): 640–649. https://doi.org/10.1061/(ASCE)CC.1943-5614.0000301

[11] M.N.S. Hadi. "The behavior of FRP wrapped HSC behavior under different eccentric loads." Composite Structures, (2005), 78 (4): 560–566. doi: 10.1016/j.compstruct.2005.11.018

[12] D. Y Wang, Z. Y. Wang, S. T. Smith, and T. Yu. "Size effect on axial stress-strain behavior of CFRP-confined square concrete columns." Construction and Building Materials, (2016), 118: 116–126. https://dx.doi.org/10.1016/j.conbuildmat.2016.04.158

[13] Concrete Society 2012. Design guidance for strengthening concrete structures using fiber composite materials: Refiber of a Concrete Society Working Party. 3rd ed. Technical Rep. No. 55. Camberley, UK: Concrete Society.

[14] Alper Ilki1, Onder Peker, Emre Karamuk, Cem Demir, and Nahit Kumbasar. "FRP Retrofit of Low and Medium Strength Circular and Rectangular Reinforced Concrete Columns". Journal of material in civil engineering, FEB-2008, pp 169-188.

[15] DOI: 10.1061/(ASCE)0899-1561(2008)20:2(169)

[16] Zhenyu Wang, Daiyu Wang, Scott T. Smith, Dagang Lu. "Experimental testing and analytical modeling of CFRP-confined large circular RC columns subjected to cyclic axial compression" Engineering Structures, (2012), 40, 64–74.

[17] http://dx.doi.org/10.1016/j.engstruct.2012.01.004

[18] Hanan Al-Nimry, Ahmad Soman. "On the slenderness and FRP confinement of eccentrically-loaded circular RC columns" Engineering Structures, (2018), 164, 92–108.

[19] https://doi.org/10.1016/j.engstruct.2018.02.086

[20] Zhong Tao, Zhi-Bin Wang, Qing Yu, Finite element modeling of concrete-filled steel stub columns under axial compression. Journal of Constructional Steel Research, (2013), 89, 121–131. http://dx.doi.org/10.1016/j.jcsr.2013.07.001

[21] Ali Khajeh Samani, Mario M. Attard. A stress–strain model for uniaxial and confined concrete under compression. Engineering Structures, (2012), 41, 335–349. http://dx.doi.org/10.1016/j.engstruct.2012.03.027

[22] Baris Binici, An analytical model for stress–strain behavior of confined concrete. Engineering Structures, (2005), 27 (7), 1040–1051. Doi :10.1016/j.engstruct.2005.03.002

[23] Najwa F. Hany, Elie G. Hantouche, Mohamed H. Harajli, Finite element modeling of FRP-confined concrete using modified concrete damaged plasticity. Engineering Structures, (2016), 125, 1–14. http://dx.doi.org/10.1016/j.engstruct.2016.06.047

[24] Yan Xiao1, Wenhui He, and Kang-kyu Choi. Confined concrete-filled tubular columns. Journal of Structural Engineering, (2005), 131 (3), 488–497. DOI: 10.1061/(ASCE)0733-9445(2005)131:3(488)

[25] J.B. Mander, M.J.N. Priestley, and R. Park, "Theoretical stress-strain model for confined concrete", Journal of Structural Engineering. (1988), 114 (8), 1804-1825.